Evidence for Direct CP Violation in $B^{\pm} \to \eta h^{\pm}$ and Observation of $B^0 \to \eta K^0$

C.-T. Hoi,[29] P. Chang,[29] H. Aihara,[44] D. M. Asner,[34] T. Aushev,[13] A. M. Bakich,[39] K. Belous,[12] V. Bhardwaj,[35] B. Bhuyan,[8] M. Bischofberger,[26] A. Bondar,[1] A. Bozek,[30] M. Bračko,[22,14] T. E. Browder,[6] M.-C. Chang,[50] Y. Chao,[29] A. Chen,[27] K.-F. Chen,[29] P. Chen,[29] B. G. Cheon,[5] K. Chilikin,[13] K. Cho,[17] Y. Choi,[38] M. Danilov,[13] Z. Drásal,[2] A. Drutskoy,[13] S. Eidelman,[1] J. E. Fast,[34] V. Gaur,[40] N. Gabyshev,[1] Y. M. Goh,[5] B. Golob,[21,14] J. Haba,[7] K. Hayasaka,[25] Y. Hoshi,[42] W.-S. Hou,[29] Y. B. Hsiung,[29] H. J. Hyun,[19] K. Inami,[25] A. Ishikawa,[43] M. Iwabuchi,[49] Y. Iwasaki,[7] T. Iwashita,[26] J. H. Kang,[49] T. Kawasaki,[32] H. J. Kim,[19] H. O. Kim,[19] J. B. Kim,[18] J. H. Kim,[17] K. T. Kim,[18] M. J. Kim,[19] K. Kinoshita,[3] B. R. Ko,[18] N. Kobayashi,[36,45] P. Kodyš,[2] S. Korpar,[22,14] P. Križan,[21,14] T. Kuhr,[16] T. Kumita,[46] Y.-J. Kwon,[49] S.-H. Lee,[18] J. Li,[37] J. Libby,[9] Z. Q. Liu,[10] R. Louvot,[20] D. Matvienko,[1] S. McOnie,[39] K. Miyabayashi,[26] H. Miyata,[32] G. B. Mohanty,[40] A. Moll,[23,41] E. Nakano,[33] M. Nakao,[7] S. Neubauer,[16] S. Nishida,[7] K. Nishimura,[6] O. Nitoh,[47] T. Ohshima,[25] S. Okuno,[15] C. W. Park,[38] H. K. Park,[19] T. K. Pedlar,[51] R. Pestotnik,[14] M. Petrič,[14] L. E. Piilonen,[48] M. Ritter,[23] M. Röhrken,[16] H. Sahoo,[6] Y. Sakai,[7] T. Sanuki,[43] O. Schneider,[20] C. Schwanda,[11] A. J. Schwartz,[3] K. Senyo,[25] M. E. Sevior,[24] M. Shapkin,[12] V. Shebalin,[1] C. P. Shen,[25] T.-A. Shibata,[36,45] J.-G. Shiu,[29] F. Simon,[23,41] P. Smerkol,[14] Y.-S. Sohn,[49] A. Sokolov,[12] E. Solovieva,[13] M. Starič,[14] M. Sumihama,[36,4] S. Tanaka,[7] G. Tatishvili,[34] Y. Teramoto,[33] K. Trabelsi,[7] M. Uchida,[36,45] T. Uglov,[13] Y. Unno,[5] S. Uno,[7] G. Varner,[6] C. H. Wang,[28] M.-Z. Wang,[29] P. Wang,[10] Y. Watanabe,[15] K. M. Williams,[48] E. Won,[18] J. Yamaoka,[6] Y. Yamashita,[31] Y. Yusa,[32] V. Zhilich,[1] and A. Zupanc[16]

(Belle Collaboration)

[1]*Budker Institute of Nuclear Physics SB RAS and Novosibirsk State University, Novosibirsk 630090*
[2]*Faculty of Mathematics and Physics, Charles University, Prague*
[3]*University of Cincinnati, Cincinnati, Ohio 45221*
[4]*Gifu University, Gifu*
[5]*Hanyang University, Seoul*
[6]*University of Hawaii, Honolulu, Hawaii 96822*
[7]*High Energy Accelerator Research Organization (KEK), Tsukuba*
[8]*Indian Institute of Technology Guwahati, Guwahati*
[9]*Indian Institute of Technology Madras, Madras*
[10]*Institute of High Energy Physics, Chinese Academy of Sciences, Beijing*
[11]*Institute of High Energy Physics, Vienna*
[12]*Institute of High Energy Physics, Protvino*
[13]*Institute for Theoretical and Experimental Physics, Moscow*
[14]*J. Stefan Institute, Ljubljana*
[15]*Kanagawa University, Yokohama*
[16]*Institut für Experimentelle Kernphysik, Karlsruher Institut für Technologie, Karlsruhe*
[17]*Korea Institute of Science and Technology Information, Daejeon*
[18]*Korea University, Seoul*
[19]*Kyungpook National University, Taegu*
[20]*École Polytechnique Fédérale de Lausanne (EPFL), Lausanne*
[21]*Faculty of Mathematics and Physics, University of Ljubljana, Ljubljana*
[22]*University of Maribor, Maribor*
[23]*Max-Planck-Institut für Physik, München*
[24]*University of Melbourne, School of Physics, Victoria 3010*
[25]*Nagoya University, Nagoya*
[26]*Nara Women's University, Nara*
[27]*National Central University, Chung-li*
[28]*National United University, Miao Li*
[29]*Department of Physics, National Taiwan University, Taipei*
[30]*Henryk Niewodniczanski Institute of Nuclear Physics, Krakow*
[31]*Nippon Dental University, Niigata*
[32]*Niigata University, Niigata*
[33]*Osaka City University, Osaka*
[34]*Pacific Northwest National Laboratory, Richland, Washington 99352*
[35]*Panjab University, Chandigarh*
[36]*Research Center for Nuclear Physics, Osaka*

[37]Seoul National University, Seoul
[38]Sungkyunkwan University, Suwon
[39]School of Physics, University of Sydney, New South Wales 2006
[40]Tata Institute of Fundamental Research, Mumbai
[41]Excellence Cluster Universe, Technische Universität München, Garching
[42]Tohoku Gakuin University, Tagajo
[43]Tohoku University, Sendai
[44]Department of Physics, University of Tokyo, Tokyo
[45]Tokyo Institute of Technology, Tokyo
[46]Tokyo Metropolitan University, Tokyo
[47]Tokyo University of Agriculture and Technology, Tokyo
[48]CNP, Virginia Polytechnic Institute and State University, Blacksburg, Virginia 24061
[49]Yonsei University, Seoul
[50]Department of Physics, Fu Jen Catholic University, Taipei
[51]Luther College, Decorah, Iowa 52101
(Received 10 October 2011; published 20 January 2012)

We report measurements of the branching fractions and CP asymmetries for $B^{\pm} \to \eta h^{\pm}$ ($h = K$ or π) and the observation of the decay $B^0 \to \eta K^0$ from the final data sample of 772×10^6 $B\bar{B}$ pairs collected with the Belle detector at the KEKB asymmetric-energy e^+e^- collider. The measured branching fractions are $\mathcal{B}(B^{\pm} \to \eta K^{\pm}) = (2.12 \pm 0.23 \pm 0.11) \times 10^{-6}$, $\mathcal{B}(B^{\pm} \to \eta \pi^{\pm}) = (4.07 \pm 0.26 \pm 0.21) \times 10^{-6}$, and $\mathcal{B}(B^0 \to \eta K^0) = (1.27^{+0.33}_{-0.29} \pm 0.08) \times 10^{-6}$, where the last decay is observed for the first time with a significance of 5.4 standard deviations (σ). We also find evidence for CP violation in the charged B modes, $A_{CP}(B^{\pm} \to \eta K^{\pm}) = -0.38 \pm 0.11 \pm 0.01$ and $A_{CP}(B^{\pm} \to \eta \pi^{\pm}) = -0.19 \pm 0.06 \pm 0.01$ with significances of 3.8 σ and 3.0 σ, respectively. For all measurements, the first and second uncertainties are statistical and systematic, respectively.

DOI: 10.1103/PhysRevLett.108.031801 PACS numbers: 13.25.Hw, 11.30.Er, 12.15.Hh

Charge-parity (CP) violation plays an important role in any explanation of the observed dominance of matter over antimatter in our Universe. Current experimental knowledge about CP violation is limited. Charmless hadronic B decays constitute sensitive probes for CP violation in the standard model (SM) as well as beyond, and can help to further elucidate this unsolved question. In the SM, the decays $B^{\pm} \to \eta^{(\prime)} K^{\pm}$ and $B^0 \to \eta^{(\prime)} K^0$ are expected to primarily proceed through $b \to s$ penguin processes and a $b \to u$ tree transition as shown in Fig. 1. The large $B \to \eta' K$ [1–3] and small $B \to \eta K$ [3,4] branching fractions can be explained by $\eta - \eta'$ mixing along with constructive and destructive interference between the amplitudes of the two penguin processes [5,6].

The branching fraction of $B^0 \to \eta K^0$ is expected to be lower than that of $B^{\pm} \to \eta K^{\pm}$, because the tree diagram in the $B^0 \to \eta K^0$ decay is color suppressed. The destructive combination of penguin amplitudes may interfere with the tree amplitude in $B \to \eta K$, resulting in a large direct CP asymmetry (A_{CP}) [5,7], defined as

$$A_{CP} \equiv \frac{\Gamma[B^- \to \eta h^-] - \Gamma[B^+ \to \eta h^+]}{\Gamma[B^- \to \eta h^-] + \Gamma[B^+ \to \eta h^+]}, \qquad (1)$$

where $\Gamma(B \to \eta h)$ is the partial width obtained for the $B \to \eta h$ decay, and h denotes K or π. Similarly, direct CP violation could be sizeable for $B^{\pm} \to \eta \pi^{\pm}$ owing to the interference between $b \to d$ penguin and $b \to u$ tree diagrams. Several theoretical calculations with different mechanisms [8–14] suggest a large A_{CP} for both $B \to \eta K$ and $B \to \eta \pi$, although the sign could be either positive or negative. Previous Belle [4] and *BABAR* [3] measurements indicate a large negative A_{CP} in $B^{\pm} \to \eta K^{\pm}$, but more data are needed to be statistically sensitive to a nonzero A_{CP} in $B^{\pm} \to \eta \pi^{\pm}$.

In this Letter, we report the first observation of $B^0 \to \eta K^0$, and evidence for direct CP asymmetries in $B^{\pm} \to \eta K^{\pm}$ and $B^{\pm} \to \eta \pi^{\pm}$ using the final Belle data set. The data sample corresponds to $(772 \pm 11) \times 10^6 B\bar{B}$ pairs collected with the Belle detector at the KEKB e^+e^- asymmetric-energy (3.5 GeV on 8.0 GeV) collider [15] operating at the $\Upsilon(4S)$ resonance. The production rates

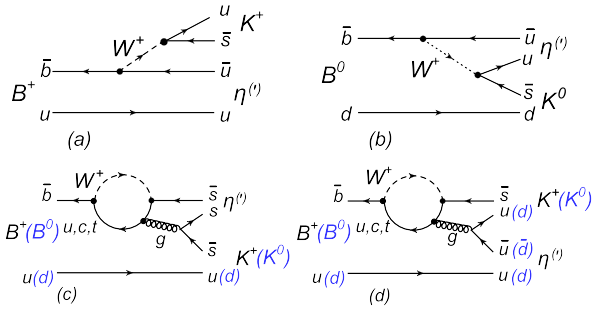

FIG. 1 (color online). (a) $b \to u$ tree diagram for $B^+ \to \eta^{(\prime)} K^+$. (b) color-suppressed $b \to u$ tree diagram for $B^0 \to \eta^{(\prime)} K^0$. (c),(d) $b \to s$ gluonic penguin diagrams for $B \to \eta^{(\prime)} K$.

of B^+B^- and $B^0\bar{B}^0$ pairs are assumed to be equal at the $\Upsilon(4S)$ resonance.

The Belle detector [16] is a large-solid-angle magnetic spectrometer that consists of a silicon vertex detector, a 50-layer central drift chamber (CDC), an array of aerogel threshold Cherenkov counters (ACC), a barrel-like arrangement of time-of-flight scintillation counters (TOF), and an electromagnetic calorimeter comprising CsI(Tl) crystals located inside a superconducting solenoid coil that provides a 1.5 T magnetic field. An iron flux-return located outside the coil is instrumented to detect K_L^0 mesons and to identify muons.

The event selection and B candidate reconstruction methods are similar to those described in Ref. [4]. We select η and π^0 candidates through the decay chains $\eta \to \gamma\gamma$ ($\eta_{\gamma\gamma}$), $\eta \to \pi^+\pi^-\pi^0$ ($\eta_{3\pi}$), and $\pi^0 \to \gamma\gamma$. We require the two photons from the η and π^0 decays to have energies ($E_{\gamma i}$, $i = 1, 2$) greater than 50 MeV. Candidate π^0 mesons are selected from pairs of photons with invariant masses between 115 MeV/c^2 and 152 MeV/c^2. In the $\eta_{\gamma\gamma}$ reconstruction, the photon energy asymmetry $|E_{\gamma 1} - E_{\gamma 2}|/(E_{\gamma 1} + E_{\gamma 2})$, is required to be less than 0.9 to reduce the large combinatorial background from low-energy photons. Photons in $\eta_{\gamma\gamma}$ reconstruction are not allowed to pair with any other photon having $E_\gamma > 100$ MeV, to form a π^0 candidate. We require the invariant mass of the $\eta_{\gamma\gamma}$ and $\eta_{3\pi}$ candidates to be in the intervals (501, 573) MeV/c^2 and (538.5, 556.5) MeV/c^2, respectively. In order to improve the π^0 and η energy resolution, a mass-constrained kinematic fit is performed after the candidate selection.

Charged tracks that come directly from the B or η decays are required to have a distance of closest approach with respect to the interaction point (IP) of less than 3.0 cm along the electron beam direction (z) and less than 0.3 cm in the transverse plane. Charged kaons and pions are identified using dE/dx information from the CDC, Cherenkov light yields in the ACC, and time-of-flight information from the TOF. This information is combined to form a likelihood ratio, $\mathcal{R}_{K/\pi} = \mathcal{L}_K/(\mathcal{L}_K + \mathcal{L}_\pi)$, where $\mathcal{L}_K$ ($\mathcal{L}_\pi$) is the likelihood of the track being a kaon (pion). Charged tracks with $\mathcal{R}_{K/\pi} > 0.6$ (< 0.4) are treated as kaons (pions) for $B^\pm \to \eta K^\pm$ ($B^\pm \to \eta\pi^\pm$) reconstruction. A less stringent requirement, $\mathcal{R}_{K/\pi} < 0.6$, is used for charged pions in the $\eta_{3\pi}$ selection. The efficiencies for the $\mathcal{R}_{K/\pi}$ requirement are 84% for kaons, 89% for pions, and 94% for pions in $\eta_{3\pi}$ reconstruction. The probability of misidentifying a kaon as a pion is 12%, while the probability of misidentifying a pion as a kaon is 6%. Furthermore, for $B^\pm \to \eta h^\pm$ and $B^0 \to \eta K^0$ we reject charged tracks consistent with either the electron or muon hypothesis.

Candidate K^0 mesons are reconstructed in $K_S^0 \to \pi^+\pi^-$ decays. The K_S^0 candidates are required to have an invariant mass lying between 488 MeV/c^2 and 508 MeV/c^2. The charged tracks for each K_S^0 candidate are required to have a distance-of-closest approach with respect to the IP of larger than 0.02 cm in the transverse plane. The angle between the K_S^0 momentum and the direction from the IP to the K_S^0 decay vertex must be within 0.03 rad. The distance between the two daughter tracks at their point of closest approach in the transverse plane is required to be less than 2.40 cm, and the flight length of the K_S^0 is required to be larger than 0.22 cm.

Candidate B mesons are identified using the modified beam-energy-constrained mass $M_{\rm bc} = \sqrt{(E^*_{\rm beam}/c^2)^2 - |\vec{p}^{\,*}_B/c|^2}$ [17], and the energy difference $\Delta E = E^*_B - E^*_{\rm beam}$, where $E^*_{\rm beam}$ is the beam energy, and E^*_B and $\vec{p}^{\,*}_B$ are the energy and modified momentum, respectively, of the B candidate in the $\Upsilon(4S)$ rest frame. The energy E^*_B is calculated as $E^*_B = E^*_\eta + E^*_h$. The momentum $\vec{p}^{\,*}_B$ is calculated according to

$$\vec{p}^{\,*}_B = \vec{p}^{\,*}_h + \frac{\vec{p}^{\,*}_\eta}{|\vec{p}^{\,*}_\eta|}\sqrt{(E^*_{\rm beam} - E^*_h)^2 - m_\eta^2}, \qquad (2)$$

where m_η is the nominal η mass [18]. Since charged tracks are generally measured with a better precision than photons, primary charged tracks from B decays have better

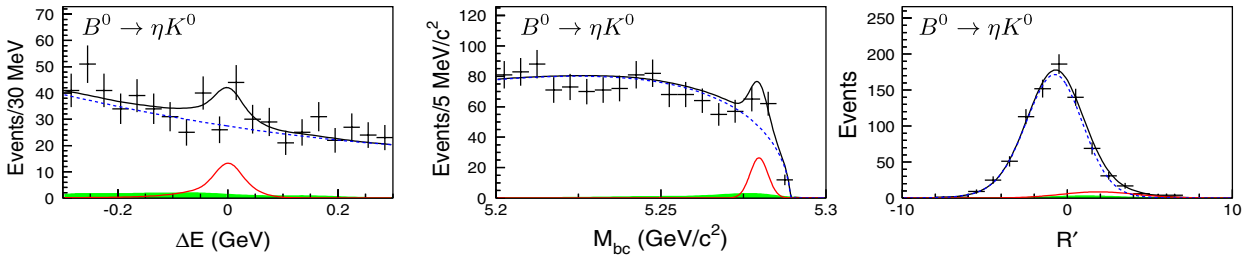

FIG. 2 (color online). ΔE (left), $M_{\rm bc}$ (middle), and $\mathcal{R}'$ (right) distributions for $B^0 \to \eta K^0$ candidate events with the $\eta_{\gamma\gamma}$ and $\eta_{3\pi}$ modes combined. Points with error bars represent the data, the total fit functions are shown by black solid curves, signals are shown by red solid curves, dashed blue curves show the continuum contributions, and filled green histograms are the contributions from charmless B backgrounds. The ΔE, $M_{\rm bc}$, and $\mathcal{R}'$ projections of the fit are for candidate events that have 5.27 GeV/$c^2 < M_{\rm bc} <$ 5.30 GeV/c^2 and $\mathcal{R}' > 0.55$, -0.10 GeV $< \Delta E < 0.08$ GeV and $\mathcal{R}' > 0.55$, and -0.10 GeV $< \Delta E < 0.08$ GeV and 5.27 GeV/$c^2 < M_{\rm bc} <$ 5.30 GeV/c^2, respectively.

momentum resolution than photons from η decays. The $\vec{p}^{\,*}_B$ resolution is improved using Eq. (2) because $\vec{p}^{\,*}_h$ and $E^*_{\rm beam}$ are determined more precisely than $\vec{p}^{\,*}_\eta$. Events with $M_{\rm bc} > 5.2$ GeV/c^2 and $|\Delta E| < 0.3$ GeV are retained for further analysis.

The dominant background arises from $e^+e^- \to q\bar{q}(q = u, d, s, c)$ continuum events. We use event topology variables to distinguish spherically distributed $B\bar{B}$ events from the jetlike continuum background. First we combine a set of modified Fox-Wolfram moments [19] into a Fisher discriminant. We then compute a likelihood from the product of probability density functions (PDFs) that describe the Fisher discriminant, $\cos\theta^*_B$, and Δz distributions. Here, θ^*_B is the angle between the B flight direction and the beam direction in the $\Upsilon(4S)$ rest frame, and Δz is the decay flight-length difference, along the z axis, between vertices of the signal B and the accompanying $\bar{B}$. A likelihood ratio, $\mathcal{R} = \mathcal{L}_s/(\mathcal{L}_s + \mathcal{L}_{q\bar{q}})$, is formed from signal ($\mathcal{L}_s$) and background ($\mathcal{L}_{q\bar{q}}$) likelihoods, which are obtained from GEANT-based [20] Monte Carlo (MC) simulated samples. Signal MC events are generated with EVTGEN [21], which invokes the PHOTOS [22] package to take final state radiation into account. We require $\mathcal{R} > 0.2$ to suppress continuum background in all modes and then translate $\mathcal{R}$ to $\mathcal{R}'$, defined as

$$\mathcal{R}' = \ln\left(\frac{\mathcal{R} - \mathcal{R}_{\rm min}}{\mathcal{R}_{\rm max} - \mathcal{R}}\right). \tag{3}$$

In this expression $\mathcal{R}_{\rm min}$ ($\mathcal{R}_{\rm max}$) is equal to 0.2 (1.0). This translation is convenient, as the $\mathcal{R}'$ distributions for signal and backgrounds can be described by a simple sum of Gaussian functions.

Signal yields are extracted by performing an unbinned extended three-dimensional maximum likelihood fit. The likelihood for each B^+ mode is defined as

$$\mathcal{L} = \frac{1}{N!}e^{-\sum_j N_j}\prod_i\left(\sum_j N_j \mathcal{P}^i_j\right),$$
$$\mathcal{P}^i_j = \frac{1}{2}[1 - q^i A_{CPj}]P_j(M^i_{\rm bc}, \Delta E^i, \mathcal{R}'^i), \tag{4}$$

where i denotes the ith event. Category j runs over the signal and background components, where background components include the continuum, the cross feed due to $K - \pi$ misidentification, and the background from other charmless B decays, but do not include $b \to c$ decays, which are found to give a negligible contribution. Here N is the sum of the number of signal and background events. The parameter N_j represents the number of events for category j, $P_j(M^i_{\rm bc}, \Delta E^i, \mathcal{R}'^i)$ is the PDF in $M_{\rm bc}$, ΔE, and $\mathcal{R}'$, and q is the B-meson charge. For the B^0 mode, the A_{CPj} parameters are set to zero since CP asymmetries cannot be determined without additional information. The validity of the three-dimensional fit is tested with large ensemble tests using MC samples and by fits to a high-statistics control sample of $B^+ \to \bar{D}^0\pi^+(\bar{D}^0 \to K^+\pi^-\pi^0)$ decays.

All the signal and cross-feed background PDFs in $M_{\rm bc}$ and $\mathcal{R}'$ are modeled with a single Gaussian. In $B \to \eta_{\gamma\gamma}h$ ($B \to \eta_{3\pi}h$) modes, the PDFs in ΔE are described by a crystal ball [23] (a sum of two Gaussians) function. The peak positions and resolutions in $M_{\rm bc}$, ΔE and $\mathcal{R}'$ are adjusted according to the data-MC differences observed in control samples [24].

The continuum background in ΔE is described by a second-order polynomial, while the $M_{\rm bc}$ distribution is parametrized with an ARGUS function, $f(x) = x\sqrt{1-x^2}\exp[-\xi(1-x^2)]$, where x is $M_{\rm bc}/E_{\rm beam}$ and ξ is a free parameter in the fit [25]. The $\mathcal{R}'$ PDF is a double

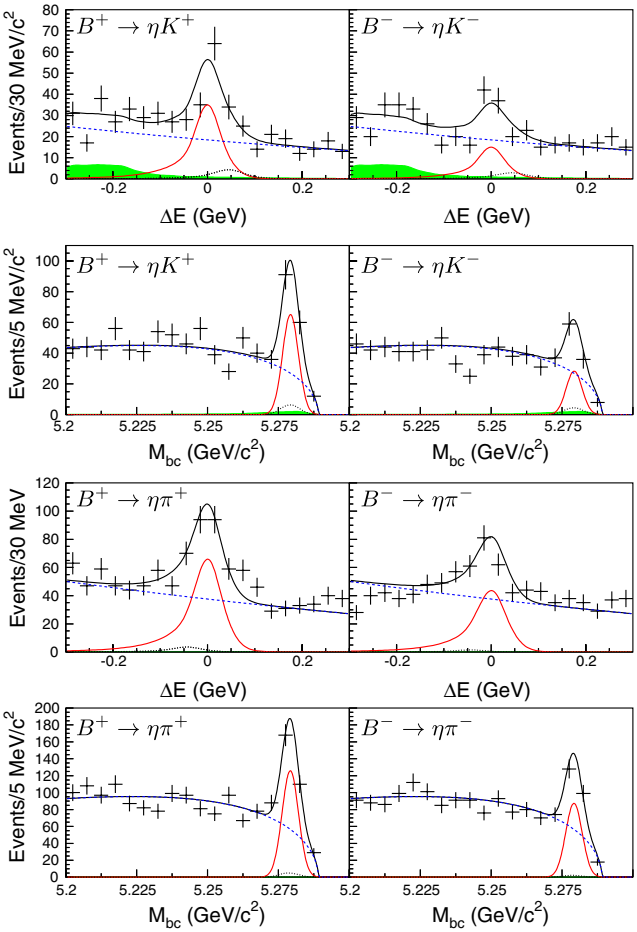

FIG. 3 (color online). ΔE and $M_{\rm bc}$ projections for $B^+ \to \eta h^+$ (left) and $B^- \to \eta h^-$ (right) candidate events with the $\eta_{\gamma\gamma}$ and $\eta_{3\pi}$ modes combined. Points with error bars represent the data, the total fit functions are shown by black solid curves, signals are shown by red solid curves, dashed curves are the continuum contributions, dotted curves are the cross-feed backgrounds from misidentification, and filled histograms are the contributions from charmless B backgrounds. The ΔE and $M_{\rm bc}$ projections of the fits are for events that have 5.27 GeV/$c^2 < M_{\rm bc} <$ 5.30 GeV/c^2 and $\mathcal{R}' > 1.95$, -0.10 GeV $< \Delta E < 0.08$ GeV, and $\mathcal{R}' > 1.95$, respectively.

TABLE I. Summary of systematic uncertainties (%) for branching fractions.

Uncertainty	$\eta_{\gamma\gamma}K^{\pm}$	$\eta_{3\pi}K^{\pm}$	$\eta_{\gamma\gamma}\pi^{\pm}$	$\eta_{3\pi}\pi^{\pm}$	$\eta_{\gamma\gamma}K^0_S$	$\eta_{3\pi}K^0_S$
π^0, η, and K^0_S reconstruction efficiencies	4.0	5.7	4.0	5.7	4.7	5.9
$\mathcal{R}(K/\pi)$ requirement	0.9	2.5	0.8	2.4	-	1.6
Tracking	0.4	1.1	0.4	1.1	0.7	1.4
$\mathcal{R}$ criterion	0.6	0.6	0.6	0.6	0.6	0.6
PDF modeling	2.4	0.9	0.8	0.3	2.0	0.8
Number of $B\bar{B}$ pairs	1.4	1.4	1.4	1.4	1.4	1.4
MC statistics	0.6	0.6	0.6	0.6	0.6	0.6
π^0, η, and K^0_S decay branching fractions	0.5	1.2	0.5	1.2	0.5	1.2
Total	5.1	6.7	4.5	6.6	5.4	6.6

Gaussian function. The background PDFs in both $M_{\rm bc}$ and ΔE for charmless B decays are modeled with smoothed two-dimensional histograms obtained from a large MC sample, and the $\mathcal{R}'$ PDF is a single Gaussian.

We perform a simultaneous fit to $B^{\pm} \to \eta K^{\pm}$ and $B^{\pm} \to \eta\pi^{\pm}$ candidate events, since these two decay modes can feed into each other. In the likelihood fits, N_j and A_{CPj} are allowed to vary for the continuum and charmless B backgrounds. Shape parameters of the continuum background PDFs are also floated. The cross-feed background in $\eta K^{\pm}$ ($\eta\pi^{\pm}$) and signal in $\eta\pi^{\pm}$ ($\eta K^{\pm}$) share the same fitting parameters in both A_{CP} and branching fraction. Figure 2 shows the $M_{\rm bc}$, ΔE and $\mathcal{R}'$ projections of the fit to the $B^0 \to \eta K^0_S$ sample. The $M_{\rm bc}$ and ΔE projections for the $B^+ \to \eta h^+$ and $B^- \to \eta h^-$ samples are shown separately in Fig. 3.

The branching fraction for each mode is calculated by dividing the efficiency-corrected signal yield by the number of $B\bar{B}$ pairs. The dominant systematic uncertainties on the branching fraction come from MC modeling of the η, π^0, and K^0_S selection efficiency; these uncertainties are 4.0%, 4.0%, and 1.6%, respectively. The systematic uncertainty due to the $\mathcal{R}(K/\pi)$ requirement is 0.9% for kaons and 0.8% for pions. It is estimated from the $D^{*+} \to D^0\pi^+(D^0 \to K^-\pi^+)$ sample. The systematic uncertainty due to the charged-track reconstruction efficiency is determined from a study of the $D^{*\pm} \to D^0\pi^{\pm}(D^0 \to \pi^+\pi^- K^0_S)$ decay. Any difference in the efficiency when the $\mathcal{R}$ criterion is applied to data or MC calculations is investigated using the $B^+ \to \bar{D}^0\pi^+(\bar{D}^0 \to K^+\pi^-\pi^0)$ sample. The fitting systematic uncertainties due to the signal PDF modeling are estimated from changes of the fit parameters while varying the calibration factors by 1 standard deviation. The systematic uncertainties on A_{CP} arise from detector bias, uncertainties on the detector bias and PDF modeling. The possible detector bias due to the tracking acceptance and $\mathcal{R}(K/\pi)$ selection for $A_{CP}(B^{\pm} \to \eta\pi^{\pm})$ is evaluated using the fitted A_{CP} value of the continuum background [26,27]. The detector bias in $A_{CP}(B^{\pm} \to \eta K^{\pm})$ is evaluated using the $D^+_s \to \phi\pi^+(\phi \to K^+K^-)$ and $D^0 \to K^-\pi^+$ samples [26,27]. There is a contribution to the A_{CP} systematic uncertainty from the modeling of the signal PDFs. Systematic uncertainties for the measured branching fraction and A_{CP} are summarized in Tables I and II, respectively.

The statistical significance is evaluated as $\sqrt{-2\ln(\mathcal{L}_0/\mathcal{L}_{\rm max})}$, where $\mathcal{L}_0$ is the likelihood value when either the signal yield or A_{CP} is fixed to zero, and $\mathcal{L}_{\rm max}$ is the nominal likelihood value. The total significance (Σ) including PDF modeling systematic uncertainty is calculated after smearing the likelihood distribution with the appropriate PDF modeling systematic uncertainties. In Table III we list the fitted signal yields, charge asymmetries, reconstruction efficiencies, and branching fractions. The combined result for the two η decay modes is obtained from the combined likelihood function.

In summary, using the final Belle data sample containing $772 \times 10^6 B\bar{B}$ pairs and a three-dimensional fit that maximizes the efficiency, we provide new measurements based on signal yields 2.5 times larger than those reported in our previous publications [4]. We find evidence for CP asymmetries in $B^{\pm} \to \eta K^{\pm}$ and $B^{\pm} \to \eta\pi^{\pm}$: $A_{CP}(B^{\pm} \to \eta K^{\pm}) = -0.38 \pm 0.11 \pm 0.01$ and $A_{CP}(B^{\pm} \to \eta\pi^{\pm}) = -0.19 \pm 0.06 \pm 0.01$. The significance of $A_{CP}(\eta K^+)$ [$A_{CP}(\eta\pi^+)$] is 3.8σ [3.0σ]. Evidence for $A_{CP}(B^{\pm} \to \eta\pi^{\pm})$ is seen for the first time. We also observe the decay $B^0 \to \eta K^0$ for the first time with a significance of 5.4σ and a branching fraction $\mathcal{B}(B^0 \to \eta K^0) = (1.27^{+0.33}_{-0.29} \pm 0.08) \times 10^{-6}$. In addition, we report the following new measurements of the branching fractions: $\mathcal{B}(B^{\pm} \to \eta K^{\pm}) = (2.12 \pm 0.23 \pm 0.11) \times 10^{-6}$ and $\mathcal{B}(B^{\pm} \to \eta\pi^{\pm}) = (4.07 \pm 0.26 \pm 0.21) \times 10^{-6}$. The result shown in Table III are consistent with Ref. [3] except for $A_{CP}(B^{\pm} \to \eta\pi^{\pm})$. All our branching fraction and A_{CP} measurements supersede the results in Ref. [4].

TABLE II. Summary of A_{CP} systematic uncertainties (10^{-2}).

Uncertainty	$\eta_{\gamma\gamma}K^{\pm}$	$\eta_{3\pi}K^{\pm}$	$\eta_{\gamma\gamma}\pi^{\pm}$	$\eta_{3\pi}\pi^{\pm}$
PDF modeling	0.8	0.8	0.6	0.4
Detector bias	0.4	0.4	0.6	1.3
Total	0.9	0.9	0.8	1.4

TABLE III. Detection efficiency (ϵ) including subdecay branching fractions, yield, significance of the yield $\Sigma(\mathcal{Y})$, measured branching fraction $\mathcal{B}$, charge asymmetry A_{CP}, and significance of the charge asymmetry $\Sigma(A_{CP})$ for $B \to \eta h$ decays. The first uncertainties are statistical and the second ones are systematic.

Mode	ϵ (%)	Yield	$\Sigma(\mathcal{Y})$	$\mathcal{B}$ (10^{-6})	A_{CP}	$\Sigma(A_{CP})$
$B^{\pm} \to \eta K^{\pm}$			13.2	$2.12 \pm 0.23 \pm 0.11$	$-0.38 \pm 0.11 \pm 0.01$	3.8
$\eta_{\gamma\gamma} K^{\pm}$	13.3	$201.9^{+27.1}_{-26.5}$	10.2	$2.07 \pm 0.27 \pm 0.10$	$-0.36 \pm 0.13 \pm 0.01$	2.9
$\eta_{3\pi} K^{\pm}$	4.9	$80.2^{+14.9}_{-13.9}$	8.6	$2.29^{+0.43}_{-0.40} \pm 0.15$	$-0.42 \pm 0.18 \pm 0.01$	2.4
$B^{\pm} \to \eta \pi^{\pm}$			22.4	$4.07 \pm 0.26 \pm 0.21$	$-0.19 \pm 0.06 \pm 0.01$	3.0
$\eta_{\gamma\gamma} \pi^{\pm}$	15.3	$480.6^{+35.1}_{-36.0}$	19.0	$4.24 \pm 0.32 \pm 0.19$	$-0.14 \pm 0.08 \pm 0.01$	1.8
$\eta_{3\pi} \pi^{\pm}$	5.4	$138.6^{+18.5}_{-17.5}$	12.2	$3.63 \pm 0.49 \pm 0.25$	$-0.31 \pm 0.13 \pm 0.01$	2.5
$B^0 \to \eta K^0$			5.4	$1.27^{+0.33}_{-0.29} \pm 0.08$		
$\eta_{\gamma\gamma} K^0$	4.2	$38.0^{+12.6}_{-11.4}$	4.0	$1.18^{+0.39}_{-0.35} \pm 0.06$		
$\eta_{3\pi} K^0$	1.5	$16.2^{+6.5}_{-5.4}$	4.1	$1.48^{+0.59}_{-0.49} \pm 0.10$		

We thank the KEKB Group for excellent operation of the accelerator, the KEK cryogenics Group for efficient solenoid operations, and the KEK computer Group and the NII for valuable computing and SINET4 network support. We acknowledge support from MEXT, JSPS and Nagoya's TLPRC (Japan); ARC and DIISR (Australia); NSFC (China); MSMT (Czechia); DST (India); MEST, NRF, NSDC of KISTI, and WCU (Korea); MNiSW (Poland); MES and RFAAE (Russia); ARRS (Slovenia); SNSF (Switzerland); NSC and MOE (Taiwan); and DOE and NSF (USA).

[1] B. H. Behrens *et al.* (CLEO Collaboration), Phys. Rev. Lett. **80**, 3710 (1998).
[2] J. Schümann *et al.* (Belle Collaboration), Phys. Rev. Lett. **97**, 061802 (2006).
[3] B. Aubert *et al.* (BABAR Collaboration), Phys. Rev. D **80**, 112002 (2009).
[4] P. Chang *et al.* (Belle Collaboration), Phys. Rev. D **75**, 071104 (2007).
[5] H. J. Lipkin, Phys. Lett. B **254**, 247 (1991).
[6] A contribution from the $b \to sgg$ diagram is considered in many theoretical approaches to explain the $B \to \eta' K$ branching fraction. Latest calculations can accommodate the large $B \to \eta' K$ branching fraction without introducing a large $b \to sgg$ contribution. The details can be found in Ref. [8] and J.-F. Hsu, Y.-Y. Charng, and H.-n. Li, Phys. Rev. D **78**, 014020 (2008).
[7] M. Bander, D. Silverman, and A. Soni, Phys. Rev. Lett. **43**, 242 (1979).
[8] H.-Y. Cheng and C.-K. Chua, Phys. Rev. D **80**, 114008 (2009).
[9] Z. J. Xiao, Z. Q. Zhang, X. Liu, and L. B. Guo, Phys. Rev. D **78**, 114001 (2008).
[10] H. S. Wang, X. Liu, Z. J. Xiao, L. B. Guo, and C. D. Lu, Nucl. Phys. **B738**, 243 (2006).
[11] A. G. Akeroyd, C. H. Chen, and C. Q. Geng, Phys. Rev. D **75**, 054003 (2007).
[12] A. R. Williamson and J. Zupan, Phys. Rev. D **74**, 014003 (2006); **74**, 039901(E) (2006).
[13] M. Beneke and M. Neubert, Nucl. Phys. **B651**, 225 (2003).
[14] C.-W. Chiang, M. Gronau, J. L. Rosner, and D. A. Suprun, Phys. Rev. D **70**, 034020 (2004).
[15] S. Kurokawa and E. Kikutani, Nucl. Instrum. Methods Phys. Res., Sect. A **499**, 1 (2003); and other papers included in this volume.
[16] A. Abashian *et al.* (Belle Collaboration), Nucl. Instrum. Methods Phys. Res., Sect. A **479**, 117 (2002).
[17] M. Nakao *et al.* (Belle Collaboration), Phys. Rev. D **69**, 112001 (2004). We follow their $M_{\rm bc}$ definition and modify it from a form for a photon to the one suitable for a massive η meson to improve the resolution for signal $M_{\rm bc}$ and to reduce the correlation between ΔE and $M_{\rm bc}$.
[18] K. Nakamura *et al.* (Particle Data Group), J. Phys. G **37**, 075021 (2010).
[19] G. C. Fox and S. Wolfram, Phys. Rev. Lett. **41**, 1581 (1978); the modified moments used in this Letter are described in S. H. Lee *et al.* (Belle Collaboration), Phys. Rev. Lett. **91**, 261801 (2003).
[20] R. Brun *et al.*, GEANT 3.21, CERN Report No. DD/EE/84-1, 1987.
[21] D. J. Lange, Nucl. Instrum. Methods Phys. Res., Sect. A **462**, 152 (2001).
[22] E. Barberio and Z. Was, Comput. Phys. Commun. **79**, 291 (1994); P. Golonka and Z. Was, Eur. Phys. J. C **45**, 97 (2006).
[23] E. D. Bloom *et al.*, Annu. Rev. Nucl. Part. Sci. **33**, 143 (1983).
[24] The ΔE peak position in the $B \to \eta_{\gamma\gamma} h$ [$B \to \eta_{3\pi} h$] decay is calibrated using the $B^+ \to \pi^0 K^+$ [$B^+ \to \bar{D}^0 \pi^+ (\bar{D}^0 \to K^+ \pi^- \pi^0)$] sample. The resolution in ΔE is adjusted using the $\bar{D}^0 \to K^+ \pi^- \pi^0$ samples. The peak positions and resolutions in $M_{\rm bc}$ and $\mathcal{R}'$ are adjusted using the $B^+ \to \bar{D}^0 \pi^+ (\bar{D}^0 \to K^+ \pi^- \pi^0)$ control sample.
[25] H. Albrecht *et al.* (ARGUS Collaboration), Phys. Lett. B **241**, 278 (1990).
[26] B. R. Ko *et al.* (Belle Collaboration), Phys. Rev. Lett. **104**, 181602 (2010).
[27] K. Sakai *et al.* (Belle Collaboration), Phys. Rev. D **82**, 091104 (2010). Since the purity of pions in the $B^{\pm} \to \eta \pi^{\pm}$ continuum component is high, we use the charge asymmetry measured in the continuum component to evaluate the charged pion detector bias. As there are protons misidentifed as kaons in the $B^{\pm} \to \eta K^{\pm}$ continuum component, we instead choose the $D_S^+ \to \phi \pi^+ (\phi \to K^+ K^-)$ and $D^0 \to K^- \pi^+$ decay samples to evaluate the charged kaon detector bias.